Rubber friction on road surfaces: Experiment and theory for low sliding speeds

B. Lorenz, Y. R. Oh, S. K. Nam, S. H. Jeon, and B. N. J. Persson

Citation: The Journal of Chemical Physics **142**, 194701 (2015); doi: 10.1063/1.4919221
View online: http://dx.doi.org/10.1063/1.4919221
View Table of Contents: http://scitation.aip.org/content/aip/journal/jcp/142/19?ver=pdfcov
Published by the AIP Publishing

Rubber friction on road surfaces: Experiment and theory for low sliding speeds

B. Lorenz,[1,a)] Y. R. Oh,[2] S. K. Nam,[2] S. H. Jeon,[2] and B. N. J. Persson[1,a)]
[1]*PGI, FZ Jülich, 52425 Jülich, Germany*
[2]*Hankook Tire Co. LTD., 112 Gajeongbuk-ro, Yuseong-gu, Daejeon 305-725, South Korea*

(Received 17 February 2015; accepted 9 April 2015; published online 15 May 2015)

We study rubber friction for tire tread compounds on asphalt road surfaces. The road surface topographies are measured using a stylus instrument and atomic force microscopy, and the surface roughness power spectra are calculated. The rubber viscoelastic modulus mastercurves are obtained from dynamic mechanical analysis measurements and the large-strain effective modulus is obtained from strain sweep data. The rubber friction is measured at different temperatures and sliding velocities, and is compared to the calculated data obtained using the Persson contact mechanics theory. We conclude that in addition to the viscoelastic deformations of the rubber surface by the road asperities, there is an important contribution to the rubber friction from shear processes in the area of contact. The analysis shows that the latter contribution may arise from rubber molecules (or patches of rubber) undergoing bonding-stretching-debonding cycles as discussed in a classic paper by Schallamach. © *2015 AIP Publishing LLC.* [http://dx.doi.org/10.1063/1.4919221]

I. INTRODUCTION

Rubber friction is a topic of great practical importance, e.g., for the tire-road interaction,[1–25] or for the friction between the rubber stopper and the barrel in syringes.[26,27] There are several different contributions to rubber friction, the relative importance of which depends on the rubber compound and countersurface properties. For hard substrates, such as road surfaces, a contribution to rubber friction arises from the time-dependent viscoelastic deformations of the rubber by the substrate asperities. That is, during sliding an asperity contact region with linear size d will deform the rubber at a characteristic frequency $\omega \sim v/d$, where v is the sliding speed. Since real surfaces have roughness over many decades in length scales, there will be a wide band of perturbing frequencies, all of which contribute to the viscoelastic rubber friction. In addition, there will be a contribution to the friction from shearing the area of real contact.

The contribution from the area of real contact can have several different origins. If a thin (say nanometer) confined fluid film, e.g., oil or wear products from the tire, or the contamination film which prevails on almost all natural surfaces, exists in the contact region then shearing this film will generate a frictional shear stress which will contribute to the rubber friction. We note that confined fluid films of nanometer thickness may have very different rheological properties than the corresponding bulk fluids.[28–30] For relative clean surfaces, direct bonding (even if mainly of the weak van der Waals type) of rubber molecules to the substrate may result in bonding-stretching-debonding cycles which result in energy dissipation (see Fig. 1). This mechanism was first considered in a pioneering work by Schallamach[31] and has recently been extended to real rubber materials by Persson and Volokitin.[32] Other contributions to the friction from the area of real contact may result from wear processes (involving bond-breaking), or the interaction between hard filler particles (usually carbon or silica particles) at the rubber surface with the countersurface. This interaction will result in wear processes where the hard filler particles scratch the countersurface (usually resulting in polishing of the countersurface[19]).

The contribution from the area of real contact to rubber friction depends sensitively on contamination particles and fluids.[33] Thus, on wet road surfaces, at high enough sliding (or rolling) speed, the surfaces in the apparent contact regions will be separated by a thin fluid film, in which case the viscoelastic deformations of the rubber give the most important contribution to the friction (see Fig. 2). Similarly, if the rubber surface is contaminated by dust particles, the interaction between the dust particles and the countersurface may give a weakly velocity independent contribution to the rubber friction coefficient (typically of order ~0.1).

Rubber friction is a complex topic and any theory for rubber friction should first be tested for the most simple situation. In this paper, we will present experimental results for the rubber friction for several rubber tread compounds and road surfaces. We consider only very small sliding speeds, from ~1 μm/s to ~1 mm/s. In this case, frictional heating results in negligible temperature increase which is important as the viscoelastic properties of rubber materials are extremely sensitive to the temperature. We also present results for several different background temperatures. The experimental results are analyzed using the Persson contact mechanics theory, and we conclude that there is an important contribution to the friction from the area of contact. The analysis shows that the latter contribution may arise from bonding-stretching-debonding cycles.

In this paper, we first present the results of the road surface topographies and power spectra (Sec. II). In Sec. III, the

[a)]www.MultiscaleConsulting.com.

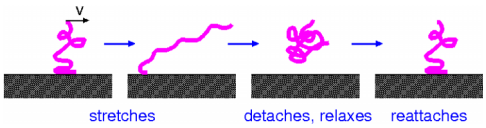

FIG. 1. The classical description of a polymer chain at the rubber-block countersurface interface. During lateral motion of the rubber block, the chain stretches, detaches, relaxes, and reattaches to the surface to repeat the cycle.[31] The picture is schematic and in reality no detachment in the vertical direction is expected, but only a rearrangement of molecule segments (in nanometer-sized domains) parallel to the surface from pinned (commensurate-like) domains to depinned (incommensurate-like) domains (see Ref. 32).

rubber viscoelastic modulus mastercurves are obtained from DMA measurements, and the large-strain effective modulus is obtained from strain sweep data. Section IV presents a short review of the theory used for analyzing the experimental friction data. In Sec. V, we present experimental rubber friction data obtained at different temperatures and velocities, and compare the measured data to the theoretical prediction. Section VI contains a discussion and Sec. VII the summary and conclusion.

II. SURFACE TOPOGRAPHIES AND SURFACE ROUGHNESS POWER SPECTRA

In this study, we use three asphalt road surfaces, denoted **a**, **b**, and **c** in what follows, and a sandpaper surface. We have observed that the asphalt road surfaces start to wear and plastically deform strongly when a rubber block is sliding on them at temperatures above 40 °C, and therefore the highest temperature used below was $T \approx 40$ °C.

We have measured the surface topography of all surfaces using an engineering stylus instrument. From the measured data, we calculated the surface roughness power spectra. To test the accuracy of the measured stylus data, we have also performed Atomic Fore Microscopy (AFM) measurements on top of some big asphalt stone particles on road surface **b**. The AFM results are consistent with the power spectrum deduced using the stylus instrument (see below), and when calculating the rubber friction (Sec. IV) we therefore use the stylus data.

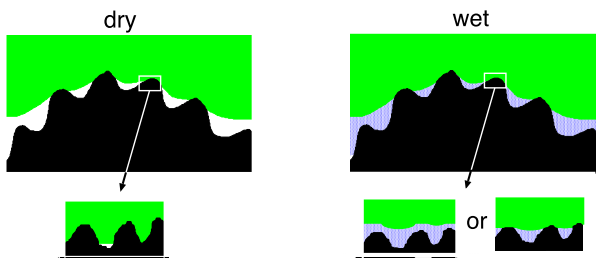

FIG. 2. With respect to the long-wavelength roughness, fluid squeeze-out from the interface between a tread block and a road surface occurs rapidly and easily and the contact mechanics appear the same as on the dry surface. However, as the magnification is increased and shorter wavelength roughness is observed, one finally observes (at some magnification ζ^*) that the rubber-road contact is separated by a thin water film which is not able to get removed because of the fluid viscosity. In this case, the adhesive contribution to rubber friction may be replaced by a contribution from shearing a thin water film, and the viscoelastic contribution may be reduced (as compared to the dry case) by the fact that the large wavevector cutoff is reduced: $q^* = \zeta^* q_0 < q_1 = \zeta_1 q_0$ (where q_1 is the cutoff wavevector on the dry surface).

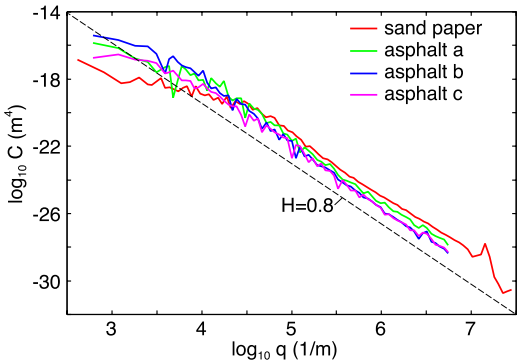

FIG. 3. The surface roughness top power spectra C_T as a function of the wavevector q ($\log_{10}$–$\log_{10}$ scale) for the asphalt road surfaces **a**, **b**, and **c**, and a sandpaper surface. The dashed line has the slope $-2(1+H) = -3.6$ corresponding to the Hurst exponent $H = 0.8$ and fractal dimension $D_f = 3 - H = 2.2$ based on 1D stylus line scan data.

Fig. 3 shows the surface roughness top power spectra C_T as a function of the wavevector q ($\log_{10}$–$\log_{10}$ scale) for the asphalt road surfaces **a**, **b**, and **c**, and for the sandpaper surface. The measurements were performed on the unused road and sandpaper surfaces, i.e., on surface areas not covered by the sliding track of the rubber block. The surfaces appear self-affine fractal with the Hurst exponent $H \approx 0.8$ (or fractal dimension $D_f = 3 - H \approx 2.2$) which is typical for many surfaces.[34] Note that the root-mean-square (rms) roughness amplitude of the sandpaper surface is smaller than for the asphalt road surfaces, but the surface roughness power spectrum at large wavevectors is largest for the sandpaper surface. This fact manifests itself in the cumulative rms roughness and rms slope curves to be presented below (see Fig. 5).

In Fig. 4, we compare the surface roughness top power spectrum C_T for the asphalt road surface **b**, obtained from the 1D stylus line scan data, with the result obtained from the 2D AFM data. The AFM data give slightly smaller power spectra which is in fact expected as the measurements were done on particular smooth surface areas on top of some big stones (the AFM cannot be used if the roughness amplitude is too high).

Fig. 5(a) shows the cumulative rms-slope and (b) the cumulative rms roughness amplitude for road surfaces **a** and **c**, and for the sandpaper surface, as a function of the logarithm of the wavevector. The cumulative rms-slope and rms-roughness

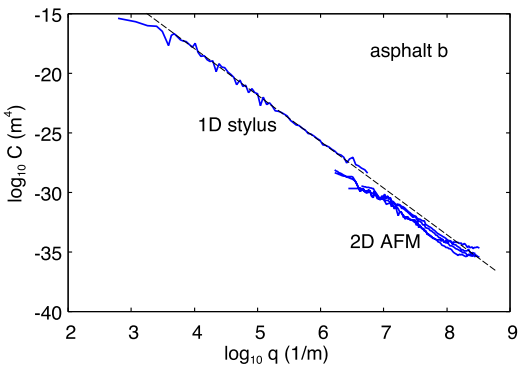

FIG. 4. The surface roughness top power spectrum C_T as a function of the wavevector q ($\log_{10}$–$\log_{10}$ scale) for the asphalt road surface **b** based on 1D stylus line scan data and 2D AFM data.

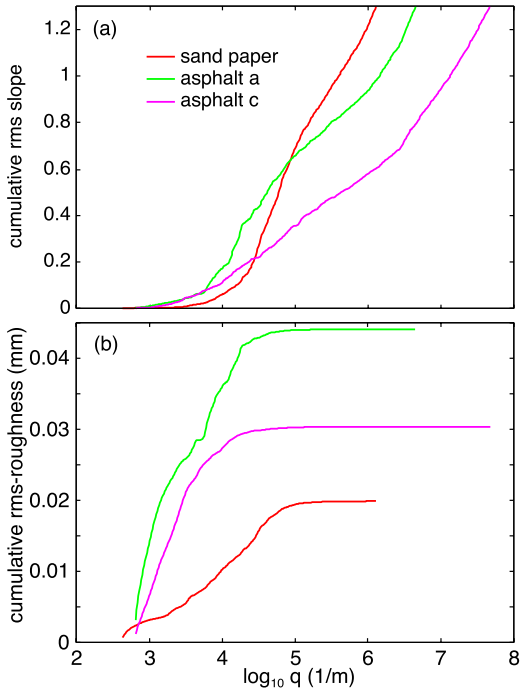

FIG. 5. (a) The cumulative rms slope and (b) the cumulative rms roughness amplitude for road surfaces **a** and **c**, and the sandpaper surface, as a function of the logarithm of the wavevector. The cumulative rms-slope and rms-roughness for a particular wavevector q is calculated including all surface roughness components with wavevector smaller than q (or wavelength longer than $\lambda = 2\pi/q$).

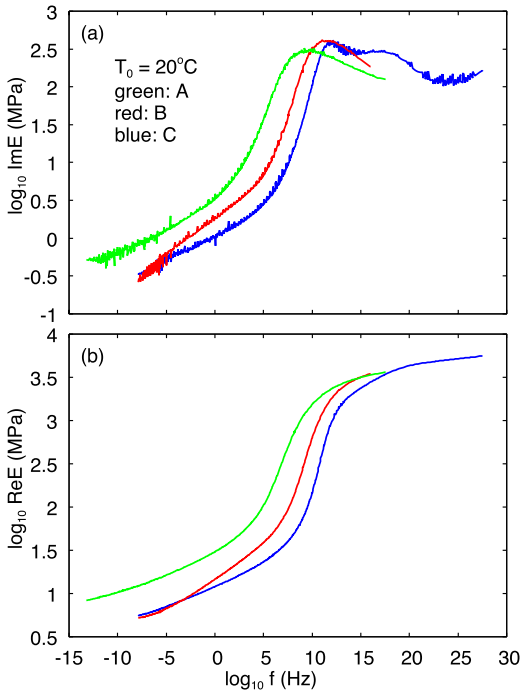

FIG. 6. The small-strain (0.04%) mastercurves for the imaginary (a) and the real (b) part of the viscoelastic modulus for compounds A, B, and C. The reference temperature $T_0 = 20\,^{\circ}\mathrm{C}$. The mastercurves have been obtained by shifting the ReE-frequency segments to form as smooth as possible mastercurve for ReE. The resulting shift factor a_T is used to obtain the mastercurves for ImE. The accuracy of the results is tested by checking that the real and imaginary parts of $E(\omega)$ obey the Kramers-Kronig relation.

amplitude for a particular wavevector q are calculated including all surface roughness components with wavevector smaller than q (or wavelength longer than $\lambda = 2\pi/q$). Note that the rms roughness amplitude is determined mainly by the longest wavelength roughness components while the rms slope depends on all, and in particular on the shorter, wavelength components. In the calculations below, we choose the large wavevector cutoff so that the rms slope including the roughness with wavevectors $q < q_1$ becomes equal to 1.3. This procedure gives $q_1 \approx 1.3 \times 10^6\ \mathrm{m}^{-1}$, $4.75 \times 10^6\ \mathrm{m}^{-1}$, and $4.7 \times 10^7\ \mathrm{m}^{-1}$ for the sandpaper surface and for the asphalt surfaces **a** and **c**, respectively. The values of q_1 for surfaces **c** are larger than for surface **a** because the former surfaces have smaller rms slope (for any given cutoff q_1), see Fig. 5.

III. RUBBER VISCOELASTIC MODULUS

We have measured the viscoelastic modulus for three rubber tread compounds A, B, and C. A is a summer compound, highly loaded with silica, B an all season compound filled with carbon black, and C is a winter compound, partially silica filled.

The viscoelastic modulus master curves were obtained from Dynamic Mechanical Analysis (DMA) measurements performed at temperatures from $-120\,^{\circ}\mathrm{C}$ to $70\,^{\circ}\mathrm{C}$ and for frequencies between 0.25 Hz and 28 Hz.

Fig. 6 shows the mastercurves (for small strain) for the imaginary (a) and the real (b) part of the viscoelastic modulus for compound A, B, and C. The reference temperature $T_0 = 20\,^{\circ}\mathrm{C}$. The mastercurves for the real and imaginary part of $E(\omega)$ in all cases obey accurately the Kramers-Kronig relation, which is a necessary condition for a linear response function, and an important test of the accuracy of the shifting procedure and measurement.[35]

Note that the viscoelastic spectra shift to higher frequencies when going from compounds A to B to C, corresponding to softer rubber with lower glass transition temperature. If we define the glass transition temperature as the temperature where $\tan\delta(T)$ is maximal (when measured at the frequency $\omega_0 = 0.01$ 1/s), we get $T_g = -39.4$, -60.3, and $-70.8\,^{\circ}\mathrm{C}$ for compound A, B, and C, respectively. The softer nature of compound C implies a larger area of contact for this compound which has important implications for the relative contributions of viscoelasticity and contact area to the friction coefficient.

We have obtained the (small-strain) mastercurves for compounds A, B, and C by shifting the ReE-frequency segments to obtain as smooth as possible mastercurve for ReE. The resulting shift factor a_T was also used when constructing the large-strain mastercurves (based on strain-sweep data obtained at $f = 1$ Hz but for many different temperatures).

In the calculations presented below, we have included strain softening by using a strain-dependent viscoelastic modulus.[36] Thus, the storage modulus is written as a product of the low-strain modulus Re$E(\omega)$ and a strain dependent factor $f(\epsilon)$ which we have measured (at different temperatures but fixed frequency) using the DMA in strain sweep mode (see above). Fig. 7 shows an example of how $f(\epsilon)$ depends on the strain ϵ (measured data). In a similar way, we multiply the low-strain loss modulus Im$E(\omega)$ with a strain dependent

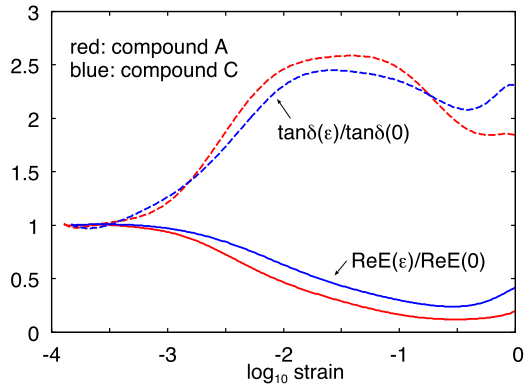

FIG. 7. The variation of $\mathrm{Re}E(\epsilon)/\mathrm{Re}E(0)$ and $\tan\delta(\epsilon)/\tan\delta(0)$ (where $\tan\delta = \mathrm{Im}E/\mathrm{Re}E$) with the $\log_{10}$ of the strain amplitude ϵ, for compounds A and C. (Note: the E-modulus was obtained using the true stress and not the engineering stress.)

factor $g(\epsilon)$. In Fig. 7, we also show the ratio $g(\epsilon)/f(\epsilon)$ with which the small-strain $\tan\delta(\omega)$ must be multiplied to account for the strain-dependency of the viscoelastic modulus.

The viscoelastic modulus $E(\omega)$ we have measured is the response to long-wavelength deformations where the rubber can be treated as homogeneous and isotropic. However, with respect to short wavelength deformations this may no longer be the case and the modulus $E(\omega,\mathbf{k})$ will also depend on the wavevector $\mathbf{k}$. We are not aware of any study of this effect, but we believe that if the shortest perturbing wavelength is larger than the filler particles (with a typical size of order 100 nm) and the important cluster size of filler particles, which typically is of order $d \approx 1$ μm (these clusters are densely packed), then using a wavevector independent E-modulus should be a good approximation. This would give a maximum wavevector of order $2\pi/d \approx 10^7$ m. This is of order the q_1 cutoff we obtain in most cases, so we believe the rubber can be described by a wavevector independent modulus.

IV. THEORY

One of us has derived a set of equations describing the friction force acting on a rubber block sliding at the velocity $v(t)$ in contact with a hard substrate with randomly rough surface.[7] In the following, the basic equations are summarized for the case of sliding at a constant velocity and neglecting heating effects due to the frictional energy dissipation. There are two contributions to the friction force, namely, (a) a contribution from the dissipation of energy inside the rubber, resulting from the viscoelasticity of the rubber material, and (b) a contribution from shearing the area of real contact. For sliding at a constant velocity v, and neglecting frictional heating, the friction coefficient due to process (a) is

$$\mu \approx \frac{1}{2}\int_{q_0}^{q_1} dq\, q^3\, C(q)S(q)P(q) \times \int_0^{2\pi} d\phi\, \cos\,\phi\, \mathrm{Im}\frac{E(qv\,\cos\,\phi,T_0)}{(1-\nu^2)\sigma_0}, \qquad (1)$$

where σ_0 is the nominal contact stress, $C(q)$ the surface roughness power spectrum, and $E(\omega,T_0)$ the rubber viscoelastic modulus. The function $P(q) = A(\zeta)/A_0$ is the relative contact area when the interface is observed at the magnification $\zeta = q/q_0$, where q_0 is the smallest (relevant) wavevector. We have

$$P(q) = \frac{2}{\pi}\int_0^\infty dx\, \frac{\sin x}{x}\exp\left[-x^2G(q)\right] = \mathrm{erf}\left(\frac{1}{2\sqrt{G}}\right), \qquad (2)$$

where

$$G(q) = \frac{1}{8}\int_{q_0}^{q} dq\, q^3C(q)\int_0^{2\pi} d\phi\left|\frac{E(qv\,\cos\,\phi,T_0)}{(1-\nu^2)\sigma_0}\right|^2. \qquad (3)$$

The factor $S(q)$ in (1) is a correction factor which takes into account that the asperity induced deformations of the rubber are smaller than would be in the case if complete contact would occur in the (apparent) contact areas observed at magnification $\zeta = q/q_0$. For contact between elastic solids, this factor reduces the elastic asperity-induced deformation energy, and including this factor gives a distribution of interfacial separation in good agreement with experiments and exact numerical studies.[37]

The interfacial separation describes how an elastic (or viscoelastic) solid deforms and penetrates into the roughness valleys, and it is these (time-dependent) deformations which cause the viscoelastic contribution to rubber friction. We assume that the same reduction factor $S(q)$ as found for elastic contact is valid also for sliding contact involving viscoelastic solids. For elastic solids, it has been found that $S(q)$ is well approximated by[38,39]

$$S(q) = \gamma + (1-\gamma)P^2(q),$$

where $\gamma \approx 1/2$. Here, we use the same expression for viscoelastic solids. Note that $S \to 1$ as $P \to 1$ which is an exact result for complete contact.

In a recent paper, Scaraggi and Persson[40] have tested the theory presented above by comparing its prediction with exact numerical results obtained for small systems. It was found that the predictions of the Persson contact mechanics theory for both the contact area A_1 and the viscoelastic friction coefficient μ_{visc}, as a function of sliding speed and nominal contact pressure, agreed very well with the result of the exact numerical simulations.

The second contribution (b) to the rubber friction force, associated with the area of contact observed at magnification $\zeta_1 = q_1/q_0$, is given by $\tau_{\mathrm{f}}A_1$. Here, $\tau_{\mathrm{f}}(v,T)$ is the (weakly) velocity and temperature-dependent effective frictional shear stress acting in the contact area $A_1 = A(\zeta_1) = P(q_1)A_0$. If we write the normal force as $F_{\mathrm{N}} = \sigma_0 A_0$, we get the total friction coefficient

$$\mu = \frac{F_{\mathrm{visc}}}{F_{\mathrm{N}}} + \frac{\tau_{\mathrm{f}}A_1}{\sigma_0 A_0} = \mu_{\mathrm{visc}} + \mu_{\mathrm{cont}}.$$

In the theory presented above enters two quantities, not directly determined by the contact mechanics theory, namely, the large wavevector cutoff q_1 and the frictional shear stress $\tau_{\mathrm{f}}(v,T)$. In order to have a complete theory for rubber friction, these quantities must be determined which requires additional information or knowledge. The cutoff q_1 is the largest surface roughness wavevector for which the rubber material behaves as a (homogeneous) viscoelastic material with the same properties as in the bulk. For dry clean surfaces, we believe that q_1 is determined by a yield criterion: when the interface is studied at higher and higher magnifications, the stresses and temperatures in the asperity contact regions increase until stress-aided,

thermally activated, bond breaking processes occur. This will result in either a thin surface layer on the rubber with different properties than the bulk (associated with mild rubber wear), or the direct removal of rubber fragments (associated with severe rubber wear), as expected for surfaces with sharp roughness such as sandpaper, where wear scars often are observed extending from one side of the rubber block to the other side.

In elastic contact mechanics, the contact area and hence the contact stresses are determined by the root-mean-square slope of the surface. We have found that if q_1 is determined by the condition that the rms slope equals 1.3 when including all the roughness components with wavevector $q_0 < q < q_1$, good agreement is obtained with experimental data for several tread rubber compounds on road surfaces.[41] In principle, the criteria for determining q_1 should also depend on the rubber properties but this effect is neglected in this approach.

Modified surface layers (thickness ≈ 1 μm) have been detected on rubber tread blocks.[42] Energy-dispersive x-ray spectroscopy analysis of the surface layer showed an increased concentration of oxygen when compared to the bulk material. The increase of oxygen in the surface region suggests that the rubber reacts chemically with the environment and is undergoing oxidation processes during sliding. This is indeed expected because of the high (flash) temperature and large stresses in the rubber road asperity contact regions during slip.

The cutoff q_1 may also be determined by road contamination particles. In this case, the cutoff q_1 may be determined by the linear size l of the contamination particles, $q_1 \approx 1/l$.

Let us now discuss the origin of the frictional shear stress $\tau_f(v,T)$ acting in the area of real contact. There are several possibilities.

(1) For clean dry surfaces, $\tau_f(v,T)$ must be due to the interactions between the rubber molecules and the substrate atoms. In many cases one expects weak interfacial interactions, e.g., the van der Waals interaction. For stationary contact, the rubber chains at the interface will adjust to the substrate potential to minimize the free energy. This bond formation may require overcoming potential barriers, and will not occur instantaneously but require some relaxation time τ^*. During sliding at low velocity, thermal fluctuations will help to break the rubber-substrate bonds resulting in a friction force which approaches zero as the sliding velocity goes to zero. At high velocity $v > D/\tau^*$ (where D is the lateral size of a pinned region; we expect D to be a few nanometer), there is not enough time for the rubber molecules to adjust to the substrate interaction potential, i.e., the bottom surface of the rubber block will "float" above the substrate forming an incommensurate-like state with respect to the corrugated substrate potential. Thus, the frictional shear stress is small also for large sliding speed. Thus, we expect the frictional shear stress as a function of the sliding speed to have a maximum at some intermediate velocity v^*. This friction mechanism was first studied in a highly simplified model by Schallamach[31] and for real rubber by Persson and Volokitin.[32] The theory predicts that the frictional shear stress is a Gaussian-like curve as a function of $\log_{10} v$ with a width of 4 (or more) frequency decades and centered at a sliding speed typically of order $v^* \sim 1$ cm/s. We will show below (see Fig. 8) that these predictions are in good qualitative agreement with what we deduce from experimental data.

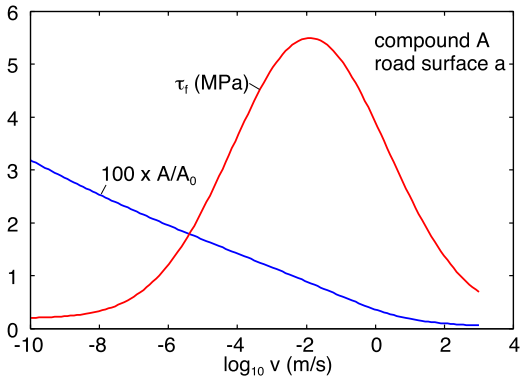

FIG. 8. Red curve: the frictional shear stress as a function of the sliding speed for the reference temperature $T_0 = 20\,^\circ$C and compound A with the glass transition temperature $T_g = -39.4\,^\circ$C. Blue curve: contact area (times a factor 100) as a function of the sliding speed. The contribution to the friction from the contact area is proportional to the product between τ_1 and A_1.

(2) There may be a contribution to μ_{cont} from interfacial crack propagation. Thus, during sliding at each substrate asperity contact region there is a closing interfacial crack on the front side (in the sliding direction) and an opening crack on the back side.[44] The energy to propagate an opening crack may be strongly enhanced by energy dissipation in the rubber in the vicinity of the opening crack, and may also enhance the contact area.[43] However, it is not clear at present how important this mechanism is when the contact regions are very small. We note that processes (1) and (2) in general will act together.

(3) There may be a contribution to rubber friction from the interaction between filler particles at the rubber surface and the road or substrate surface. Basically, during slip the hard filler particles could scratch the road surface. This may give a nearly velocity independent background contribution to the rubber friction coefficient, which will depend on the filler concentration (which is usually rather high, of order ~50% of the rubber compound volume), which may typically be of order $\mu \sim 0.1$. In the future we want to analyze this friction mechanism by performing sliding friction experiments on (very smooth) glass and PMMA (plexiglass) surfaces and study the surface topography using AFM. If we observe scratches on the substrate surfaces we know that filler particles will contribute to the rubber friction coefficient and we will be able to estimate the contribution to the friction using model experiments. It would be useful to use both filled and unfilled rubber and as filler use both carbon black and silica as these particles may have different hardness.

(4) If contamination fluids (e.g., fragments of rubber molecules or oil from the rubber) occur at the sliding interface, process (1) may be replaced by shearing a thin (say nanometer) fluid film. Here, we note that the rheological properties of such nanometer thick confined fluid films are very different from the bulk liquids. Thus, experiments[30] and theory[28] show that the frictional shear stress depends only very weakly on the shear rate and different liquids

exhibit similar properties with $\tau_f \approx B\dot{\gamma}^\alpha$ (where $\dot{\gamma}$ is the shear rate, e.g., for Couette flow $\dot{\gamma} = v/d$, where d is the film thickness), where the index $\alpha \approx 0.1$ and (if τ_f and $\dot{\gamma}$ are in SI units) $B \approx 10^5$ for many liquids at room temperature. This is in sharp contrast to Newtonian liquids where $\alpha = 1$.

(5) If contamination particles, e.g., stone dust, occur, the frictional shear stress in the contact area may be similar to that of hard material sliding on hard material, e.g., stone on stone. This situation is similar to the influence filler particles may have on the frictional shear stress.

(6) There will be a contribution to the friction from rubber wear processes. This may be particularly important for rubber sliding on sandpaper (and other surfaces with sharp surface roughness) where strong wear occurs and where one often can observe wear scars extending from one side of the rubber block to the other side as a result of the cutting action by the sharp substrate asperities. Grosch has stated (estimated) that rubber wear gives a negligible contribution to the friction,[45] but taking into account that rubber wear usually occurs by crack propagation in the rubber, and that the crack propagation energy $G(v)$ may be strongly enhanced by bulk viscoelasticity, it is not clear to us that this statement is true for surfaces with sharp roughness. We therefore plan to measure the wear rate and the size of rubber wear particles to estimate the contribution to the friction from wear processes, assuming the particles are removed by crack propagation. We also note that the energy needed to form the thin layer of modified rubber often observed on rubber surfaces may contribute to rubber friction. However, if this layer forms mainly as a result of frictional heating then it would influence the friction only indirectly by changing the rubber surface viscoelastic (and other) properties.

V. RUBBER FRICTION: EXPERIMENTAL AND THEORY RESULTS

We now present experimental results for rubber friction for compounds A, B, and C on asphalt road surfaces **a** and **c** and the sandpaper surface. We also performed measurements on the road surface **b** but the surface was destroyed when friction measurements were performed at ≈40 °C and no results for this surface will be reported on here. The experimental data will be analyzed using the Persson rubber friction theory, where there are two contributions to the friction, namely, (a) from viscoelastic energy dissipation in the rubber and (b) from shearing the area of real contact. We use the following procedure to calculate the total friction force.

(a) The cutoff q_1 is determined by the condition that including all the roughness components up to the cutoff q_1 results in the (cumulative) rms-slope 1.3.

(b) We use a frictional shear stress $\tau_f(v,T)$ in the area of contact which depends on the sliding speed v and the temperature T. The function $\tau_f(v,T)$ was deduced in an earlier study by comparing the measured friction coefficient to the calculated value.[46]

We now describe how the frictional shear-stress law $\tau_f(v,T)$ was obtained in Ref. 46. Using the same procedure as above, we first determined the q_1 cutoff for road surface **a**. Next, using the Persson contact mechanics theory for a tread compound (which we denote as compound A′ in what follows) on road surface **a**, we first calculated the viscoelastic contribution μ_{visc} to the friction coefficient and the area of contact A_1 including all the roughness up to the cutoff q_1. The total friction coefficient is

$$\mu = \mu_{visc} + \frac{\tau_f A_1}{\sigma_0 A_0}.$$

Thus, we can calculate τ_f from the measured friction coefficient μ_{exp} using

$$\tau_f = (\mu_{exp} - \mu_{visc})\frac{\sigma_0 A_0}{A_1}. \quad (4)$$

For compound A′ on road surface **a**, we measured the friction coefficient for 5 different temperatures and calculated $\tau_f(v)$ for all 5 temperatures using (4). It turned out that it is possible to shift the different measured $\tau_f(v)$ segments along the velocity axis to form a smooth mastercurve. The shear stress τ_f was well approximated by a Gaussian function of $\log_{10} v$ given by

$$\tau_f = \tau_{f0}\ \exp\left(-c\left[\log_{10}\left(\frac{v}{v_0}\right)\right]^2\right), \quad (5)$$

where $c = 0.1$, $v_0 = 6 \times 10^{-3}$ m/s, and $\tau_{f0} = 6.5$ MPa. The frictional mastercurve for compound A is shown in Fig. 8. The full width at half-maximum of the $\tau_f(v)$ as a function of $\log_{10} v$ is $2(\ln 2/c)^{1/2} \approx 5.3$.

We note that a very similar frictional shear stress law as found above (Eq. (5) and Fig. 8) has been observed (measured) by Grosch[3,4] for rubber sliding on smooth surfaces (glass or steel), and also obtained by one of us in theoretical studies of the adhesive contribution to the frictional shear stress for smooth surfaces.[32]

The mastercurve (5) is for the reference temperature T_{ref} = 20 °C but the frictional shear stress at other temperatures can be obtained by replacing v with va_T', where a_T' is the shift factor obtained when constructing the mastercurve (5). In Ref. 46 we found that the shift factor a_T' is well described by the Arrhenius factor and that the same friction mastercurve (5) could be used for all three compounds A′, B′, and C′ with very different glass transition temperatures (T_g = −38, −55, and −66 °C) assuming we use the following T_g-dependent (Arrhenius type) shift factor:

$$\ln\ a_T' = \frac{\epsilon}{k_B}\left(\frac{1}{T} - \frac{1}{T_0} - \frac{1}{T_g} + \frac{1}{T_{g0}}\right), \quad (6)$$

where $\epsilon \approx 0.94$ eV is the activation energy, $T_0 = 273.0 + 20.0$ K is the (reference temperature), and $T_{g0} = 273.0 - 38.0$ K the glass transition temperature for the compound A′. Using this law, we can calculate the frictional shear stress $\tau_f(v,T) = \tau_f(a_T'v)$ for any rubber compound, temperature, and sliding speed. In Ref. 46 we have shown how law (5) + (6) together with Persson's contact mechanics theory could reproduce the observed friction coefficient for three compounds on three surfaces and for several temperatures.

For compound A used in the present study, in Fig. 9 we show the shift factor a_T' (red line) and the shift factor a_T associated with the bulk viscoelastic modulus (blue line). Note

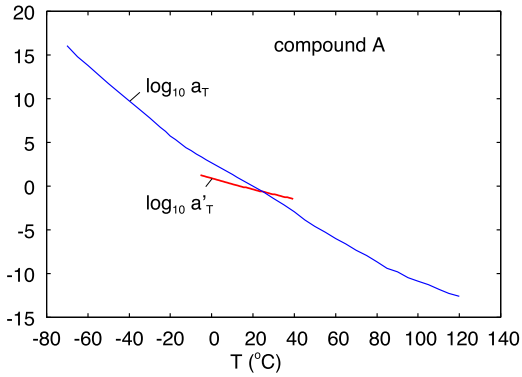

FIG. 9. The red line is the shift factor a'_T for the frictional shear stress for compound A on road surfaces **a**. The blue curve is the (bulk) viscoelastic shift factor a_T of compound A.

that the bulk viscoelastic modulus exhibits a much stronger temperature dependency than the frictional shear stress τ_f (the slope of the red and blue lines around the reference temperature correspond to activation energies ≈1 and ≈2 eV, respectively).

We can write (6) of the form

$$\ln\, a'_T = C'_1\left(\frac{1}{T} - \frac{1}{T_g} + C'_2\right), \tag{7}$$

where $C'_1 = 1.1\times 10^4$ K and $C'_2 = 8.4\times 10^{-4}$ K^{-1}. We have found that using these values for C'_1 and C'_2 we obtain good agreement with a large set of measured friction data. Nevertheless, one cannot expect C'_1 and C'_2 to be universal constants, but they will depend slightly on the rubber compound. The situation is similar to the (bulk viscoelasticity) Williams-Landel-Ferry (WLF) shift factor[47]

$$\log_{10} a_T = \frac{-C_1(T-T_g)}{C_2 + T - T_g}.$$

For many polymers $C_1 \approx 15$ and $C_2 \approx 50$ K, but these values are not universal as they depend slightly on the polymer used.

We also find that the maximum τ_{f0} in the $\tau_f(v)$ relation varies slightly depending on the studied system. Thus, for τ_{f0} we used slightly different values for different compounds and road surfaces but always in the range $\tau_{f0} = 5.3 - 8.3$ MPa.

To summarize, in Ref. 46 we measured the friction coefficient $\mu(v,T)$ for 9 surface-tread compound combinations (three road surfaces **a**, **b**, and **c** and three rubber compounds A′, B′, and C′), and using (4) and (2) we found good agreement with the theory predictions for all cases. In the present study, we show that the same frictional shear-stress law can describe the observed velocity and temperature dependency of the friction coefficient for compounds A, B, and C, which is a beautiful and remarkable result. In some cases, we add to the calculated friction coefficient a small constant contribution μ_a of order 0.1. This contribution may be derived from the interaction between the filler particles and the road surface.

In Fig. 10 we show the calculated [using (5) and (6)] total friction coefficient (solid lines) and the contribution to the friction from the area of real contact (dashed lines) for compound A (glass transition temperature $T_g = -39.4$ °C) on road surface **a**. The square symbols are the measured friction coefficients for the temperatures (a) 39.4 °C, (b) 19.0 °C, and (c) −6.5 °C.

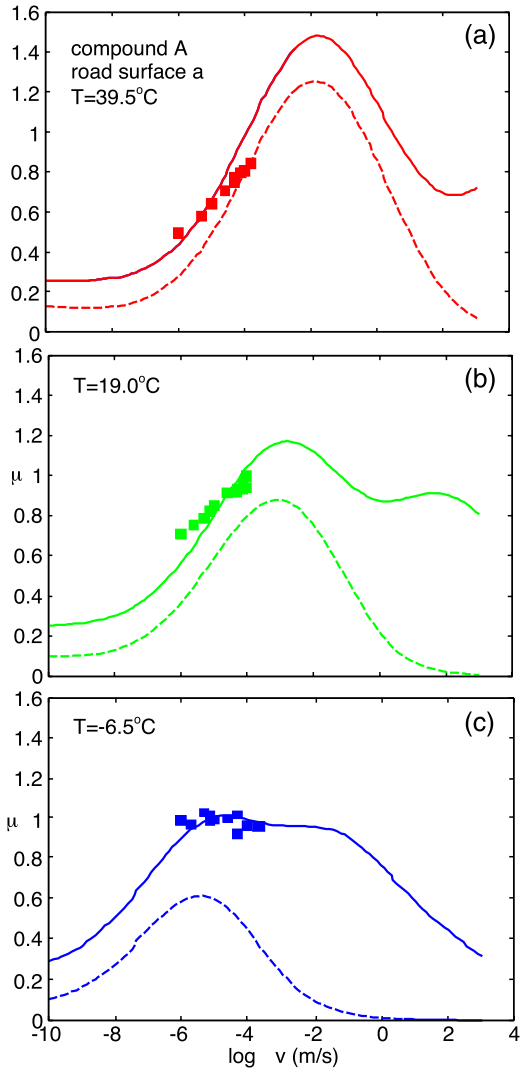

FIG. 10. The calculated total friction coefficient (solid lines) and the contribution to the friction from the area of real contact (dashed lines) for compound A on road surface **a**. The square symbols are the measured friction coefficients for the temperatures (a) 39.4 °C, (b) 19 °C, and (c) −6.5 °C. In all cases $T_g = -39.4$ °C, $\tau_{max} = 5.3$ MPa, and $\mu_a = 0.05$.

For the other two compounds, equally good agreement between theory and experiment prevails if we use in (7) a slightly different value for C'_2 than given above. However, we find it more pedagogical to instead of changing C'_2 we express the modification as a small shift in the glass transition temperatures. Thus, in Fig. 11 we show the calculated total friction coefficient (solid lines) and the contribution to the friction from the area of real contact (dashed lines) for compound B on road surface **a**. The square symbols are the measured friction coefficients at room temperature. In the calculation we have used $T_g = -53$ °C which is about 7 °C higher than deduced from the bulk viscoelastic modulus (−60.3 °C). Alternatively, if we keep T_g as the measured (bulk) glass transition temperature we need to use in (7) $C'_2 = 6.9\times 10^{-4}$ K^{-1} instead of $C'_2 = 8.4\times 10^{-4}$ K^{-1}.

Figs. 12-16 show the comparison between the measured and calculated friction coefficients for several other compound-countersurface combinations and in Table I we summarize the parameters used in the calculations.

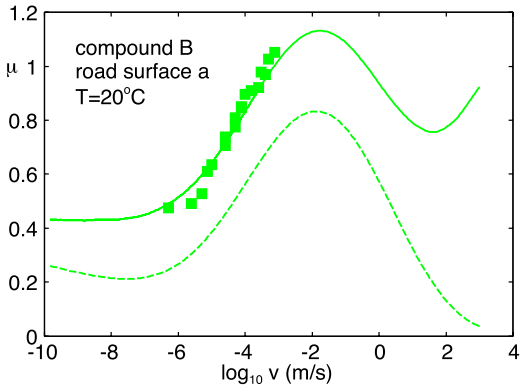

FIG. 11. The calculated total friction coefficient (solid lines) and the contribution to the friction from the area of real contact (dashed lines) for compound B on road surfaces **a**. The square symbols are the measured friction coefficients at room temperature. In the shift factor a'_T (Eq. (6)) we have used $T_g = -53\,^\circ\text{C}$ which is about 7 °C higher than the bulk glass transition temperature, and using $\tau_{max} = 6.5$ MPa and $\mu_a = 0.15$.

Let us briefly discuss how roughness on different length scales contributes to the friction and also how the area of real contact depends on the sliding velocity. Fig. 17 shows the calculated cumulative viscoelastic contribution to the friction coefficient for compounds A, B, and C on road surfaces **a** at room temperature. In the calculation of $\mu_{visc}(q_1)$ only the surface roughness components with $q < q_1$ are included. Note that there is a negligible contribution from the roll-off region in the surface roughness power spectrum which for all surfaces

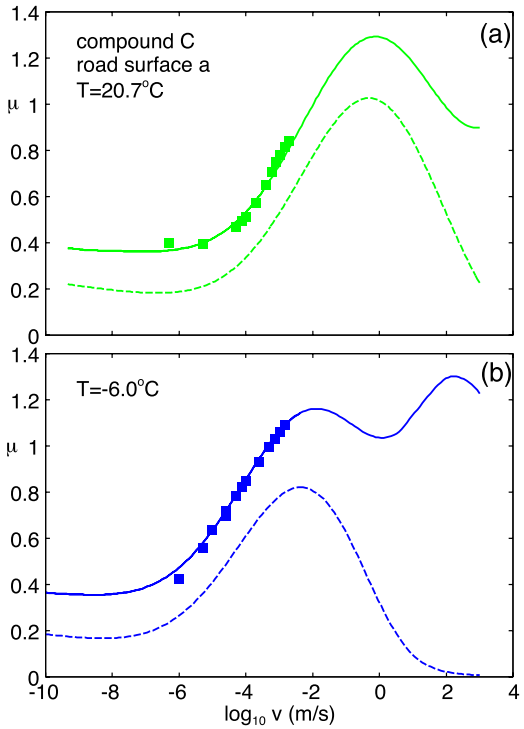

FIG. 12. The calculated total friction coefficient (solid lines) and the contribution to the friction from the area of real contact (dashed lines) for compound C on road surface **a**. The square symbols are the measured friction coefficients for the temperatures (a) 20.7 °C and (b) −6.0 °C. In the shift factor a'_T (Eq. (6)) we have used $T_g = -65\,^\circ\text{C}$ which is about 6 °C higher than the bulk glass transition temperature, and using $\tau_{max} = 6.5$ MPa and $\mu_a = 0.15$.

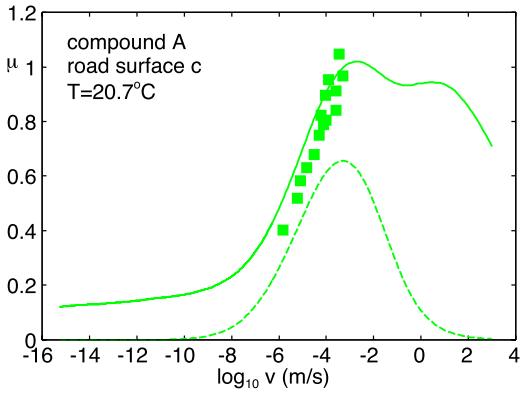

FIG. 13. The calculated total friction coefficient (solid lines) and the contribution to the friction from the area of real contact (dashed lines) for compound A on road surface **c**. The square symbols are the measured friction coefficients for room temperature and with $T_g = -39.4\,^\circ\text{C}$, $\tau_{max} = 5.3$ MPa, and $\mu_a = 0$.

occurs for $q < q_r \approx 10^{3.8}$ m^{-1} (see Fig. 3). Note also that for surface roughness with wavevector larger than the q_r each decade in length scale contributes roughly equally to the total friction coefficient.

Fig. 18 shows the calculated area of contact A_1 (in units of the nominal contact area A_0) for compounds A, B, and C on road surfaces **a** as a function of the sliding velocity. For room temperature and the nominal contact pressure, $\sigma_0 = 0.065$ MPa. In tire applications the nominal contact pressure is about $\sigma_0 \approx 0.4$ MPa, i.e., about 6 times higher than used above, and the area of real contact in this case will also be ≈6 times higher than shown in this figure.

Another interesting quantity is the mean separation $\bar{u}$ between the rubber and road surface, which depends on the road surface, rubber compound, sliding speed, temperature, and nominal contact pressure. As an example, for compound B on asphalt road surface **a** at $T = 20\,^\circ\text{C}$, for the nominal contact pressure 0.065 MPa (used in our experiments) and the sliding speed 1 m/s, the mean separation is $\bar{u} \approx 80$ μm. At the nominal contact pressure 0.3 MPa (typical in tire applications) we instead get $\bar{u} \approx 40$ μm, which is of order the rms roughness amplitude of the surface (note: the difference between the

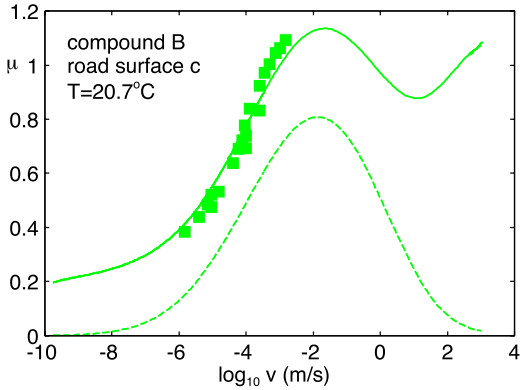

FIG. 14. The calculated total friction coefficient (solid lines) and the contribution to the friction from the area of real contact (dashed lines) for compound B on road surface **c**. The square symbols are the measured friction coefficients at room temperature. In the shift factor a'_T (Eq. (6)) we have used $T_g = -53\,^\circ\text{C}$ which is about 7 °C higher than the bulk glass transition temperature, and using $\tau_{max} = 8.5$ MPa and $\mu_a = 0$.

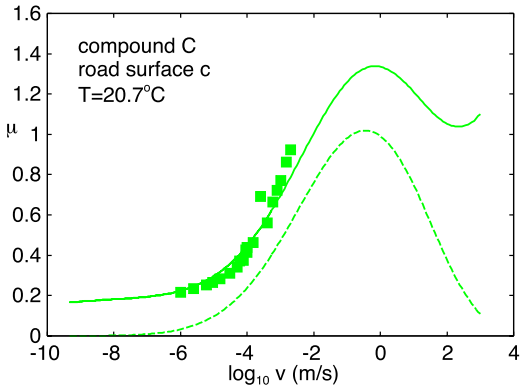

FIG. 15. The calculated total friction coefficient (solid lines) and the contribution to the friction from the area of real contact (dashed lines) for compound C on road surface **c**. The square symbols are the measured friction coefficients for room temperature and with $T_g = -65\,^\circ$C which is about 6 °C higher than the bulk glass transition temperature, and using $\tau_{max} = 8.5$ MPa and $\mu_a = 0$.

highest and lowest point in the surface is typically ∼10 times higher than the rms roughness amplitude). At higher sliding speed (neglecting frictional heating) or lower temperature the rubber is effectively stiffer and $\bar{u}$ larger.

Finally, we emphasize that the measured friction coefficients reported above were obtained by averaging the measured friction force over the length of the sliding track (about 5-10 cm). However, the friction force fluctuates irregularly along the sliding track depending on the exact location on the road surface. If the rubber block nominal contact area (and the load) would be larger, these fluctuations would be smaller (average out).

VI. DISCUSSION

We note that there is no way to obtain the measured friction coefficient assuming only a viscoelastic contribution to the friction. That is, even if q_1 is chosen as large as physically possible, namely, of order $2\pi/a \approx 10^{10}$ m^{-1}, where a is an atomic length scale, it is not possible to obtain so high friction coefficient in the low velocity region ($v \approx 10^{-3}$ m/s) as observed in the experiments. It is possible that there remains

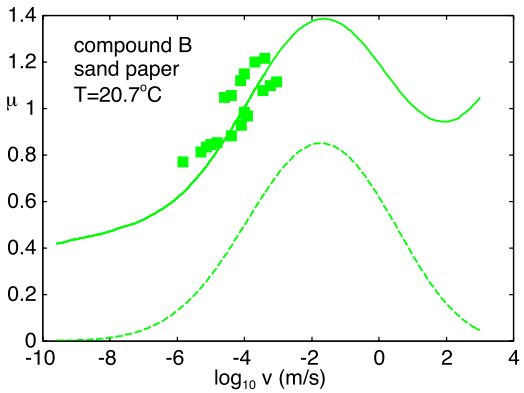

FIG. 16. The calculated total friction coefficient (solid lines) and the contribution to the friction from the area of real contact (dashed lines) for compound B on a sandpaper surface. The square symbols are the measured friction coefficients at room temperature. In the shift factor a'_T (Eq. (6)) we have used $T_g = -53\,^\circ$C which is about 7 °C higher than the bulk glass transition temperature, and using $\tau_{max} = 6.5$ MPa and $\mu_a = 0.25$.

TABLE I. Summary of parameters used in the friction calculations. A, B and C denote the rubber compounds, and **a**, **b** and **c** the asphalt road surfaces and **s** the sand paper surface. τ_{f0} is the maximum of the frictional shear stress and μ_a a constant friction coefficient added to the total friction coefficient.

Compound-surface	τ_{f0} (MPa); μ_a	T_g (°C) used (bulk)
A-**a**	5.3; 0.05	−39.4 (−39.4)
B-**a**	6.5; 0.15	−53.0 (−60.3)
C-**a**	6.5; 0.15	−65.0 (−70.8)
A-**c**	5.3; 0.00	−39.4 (−39.4)
B-**c**	8.5; 0.00	−53.0 (−60.3)
C-**c**	8.5; 0.00	−65.0 (−70.8)
B-**s**	6.5; 0.25	−53.0 (−60.3)

some viscoelastic contribution in the part we now denote as the contribution from the area of real contact (or the adhesive contribution), but the major part must be of different nature.

The frictional shear stress $\tau_f(v,T)$ used above (see Fig. 8) is consistent with what was observed by Grosch when sliding rubber on smooth substrates (glass and steel). If the substrate is perfectly smooth, there is no contribution from viscoelastic deformations by the substrate asperities and the total friction is due to shearing the area of real contact.[48] In Fig. 19, we show the friction coefficient measured by Grosch for acrylonitrile-butadiene rubber on smooth glass as a function of the logarithm of the sliding speed. The reference temperature $T_{ref} = 20\,^\circ$C. The relation between μ and $\log_{10} v$ is Gaussian-like with a full width at half-maximum of approximately 6 velocity decades which is similar to our results (see Fig. 8) having a full width at half-maximum of about 5 velocity decades. The maximum of the $\mu(v)$ function in Fig. 19 occurs for $v \approx 10^{-3}$ m/s which is close to our result (Fig. 8) (note: the reference temperature is in both cases 20 °C and the glass rubber transition temperatures are similar so that the curves can be directly compared).

As discussed in Sec. V we have found that the adhesive contribution to rubber friction exhibits a different temperature dependency than the viscoelastic contribution. In Ref. 49, Klüppel *et al.* have studied rubber friction and found that friction mastercurves can be obtained using the bulk viscoelastic shift factor a_T. This result is indeed expected if the contribution from the area of (apparent) contact is absent, as would be the case if the surfaces are separated by a thin fluid film every-

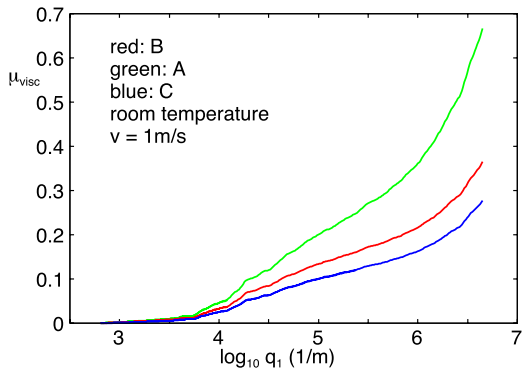

FIG. 17. The calculated cumulative viscoelastic contribution to the friction coefficient for the sliding speed $v = 1$ m/s for compounds A, B, and C on road surface **a**. In the calculation of $\mu_{visc}(\zeta)$, only the surface roughness components with $q < q_1$ are included.

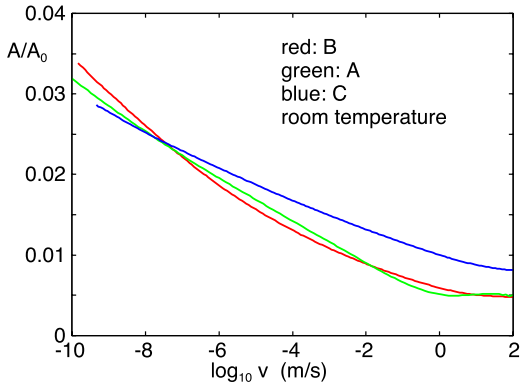

FIG. 18. The calculated area of contact A_1 (in units of the nominal contact area A_0) for compounds A, B, and C on road surfaces **a** for room temperature and the nominal contact pressure, $\sigma_0 = 0.065$ MPa. In tire applications, the nominal contact pressure is about $\sigma_0 = 0.4$ MPa, i.e., 6 times higher and therefore the area of real contact will also be ≈6 times higher than shown in this figure.

where. Grosch claims that even for dry surfaces he could form smooth friction mastercurves by shifting the $\mu(v)$ segments measured at different temperatures using the bulk viscoelastic shift function. For the sandpaper surfaces he used in most of his studies this may be due to large wear processes: the frictional shear stress in the area of contact may be determined mainly by the energy to remove rubber fragments which involves crack propagation. Crack propagation in rubber exhibits the same temperature dependency as the bulk viscoelastic modulus, as has been shown by Gent[50] and also predicted by theory.[51–53]

The frictional shear stress found above can be understood in a picture (see Fig. 1) involving a polymer chain in contact with a lateral moving countersurface. The chain stretches, detaches, relaxes, and reattaches to the surface to repeat the cycle. In each cycle, energy is dissipated resulting in a friction force. This process can be modeled theoretically as first done by Schallamach[31] and in greater detail by one of us (see Ref. 32), where a more accurate (or realistic) picture of the frictional shear process was used.

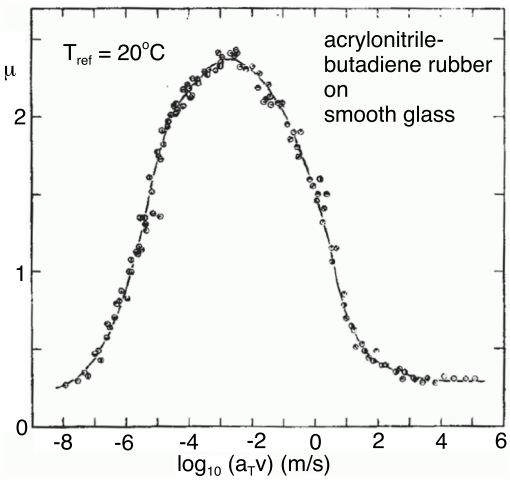

FIG. 19. The friction coefficient as a function of the (temperature-renormalized) sliding speed[3] for acrylonitrile-butadiene rubber on smooth glass. The reference temperature is $T_{ref} = 20$ °C.

The velocity dependency of the frictional shear stress shown in Fig. 8 can be understood based on the theory of thermally activated, stress aided processes. Thus, at very low sliding speed (on the left side of the maximum of the $\tau_f(v)$ curve in Fig. 8) the elongation of a rubber-substrate bond occurs slowly, and in this case there is enough time for a high-energy thermal fluctuation to occur which will supply the energy necessary to break the rubber-substrate bond. In this case, the elongation of the rubber-substrate bond is very small and very little energy is lost in the relaxation of the stretched chain upon detachment. At very high sliding speed (on the right side of the maximum of the $\tau_f(v)$ curve in Fig. 8) there is no time for a detached rubber molecule segment to adjust to the substrate potential and find a good binding position on the substrate surface. In this case, there are almost no (localized) bonds formed between the rubber and the substrate resulting in almost vanishing frictional shear stress. The maximum in the $\tau_f(v)$ curve occurs between the velocities where these two limiting cases prevail.

The magnitude of the frictional shear stress found above with a maximum value of order 6-8 MPa is consistent with experimental observations for smooth surfaces, where there is no or negligible contribution from asperity induced viscoelastic energy dissipation. Thus, for example, the frictional shear stress between a rubber stopper and a glass or polymer barrel (unlubricated) is typically a few MPa at sliding velocities $\sim 10^{-2}$ m/s. As another example, Krick *et al.* have measured the frictional shear stresses when sliding a carbon black filled natural rubber ball on smooth glass surfaces.[54] Again the frictional shear stress is of order a few MPa at sliding speeds of order ~1 m/s.

The surfaces used in this study were very often cleaned using a brush. However, experiments performed later for other rubber-road systems have shown that the maximum in the adhesive contribution depends on how clean the surfaces are. Thus, cleaning the road surfaces by brushing them in warm soap water for long time and then drying the surface results in a larger maximum adhesive contribution to the friction coefficient. When the surface is kept in the normal atmosphere for a few days, the maximum friction decreases towards the original value found before the extensive cleaning of the surface. Real road surfaces may of course be strongly contaminated, and in this case the adhesive contribution will be even smaller. It is

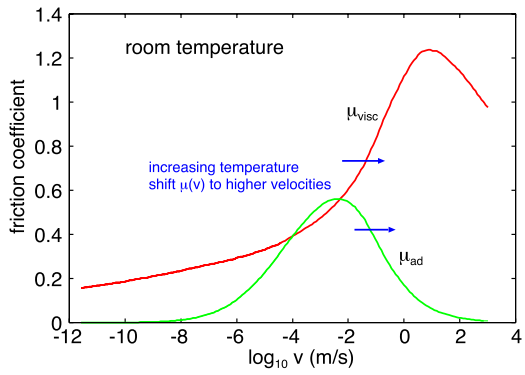

FIG. 20. Schematic picture illustrating that an increase in the temperature shifts both $\mu_{cont}(v)$ and $\mu_{visc}(v)$ towards higher sliding speeds.

in fact well known that road surfaces after raining typically exhibit (in the dry state) higher friction coefficients than before the raining started. Clearly, the role of contamination is very important and requires more studies.

We note that at room temperature, the maximum in the adhesive contribution is located below the typical slip velocities in tire applications (1-10 m/s) while the maximum in the viscoelastic contribution may be located above typical sliding speeds as is indicated in Fig. 20. Increasing the temperature shifts both $\mu_{\rm cont}(v)$ and $\mu_{\rm visc}(v)$ towards higher sliding speeds, and also increases the contact area A_1, making the adhesive contribution more important at typical sliding speeds.

VII. SUMMARY AND CONCLUSION

We have measured the rubber friction for three tire tread compounds on two asphalt road surfaces and on a sandpaper surface. The study was performed at low sliding speed $v < 1$ mm/s in order to be able to neglect frictional heating but for several different background temperatures. The road surface topographies were measured using a stylus instrument and AFM. The rubber viscoelastic modulus mastercurves were obtained from DMA measurements and the large-strain effective modulus is obtained from strain sweep data. The Persson contact mechanics theory was used to analyze the experimental data. We conclude that in addition to the viscoelastic deformations of the rubber surface by the road asperities, there is an important contribution to the rubber friction from shear processes in the area of contact. The analysis showed that the latter contribution may arise from bonding-stretching-debonding cycles as first discussed in a classic paper by Schallamach. We have proposed a simple law for how the frictional shear stress $\tau_{\rm f}(v,T)$ acting in the contact area depends on the sliding speed v and the temperature T. The temperature dependency is described by an Arrhenius-like shift factor a_T' which, in the same spirit as the WLF shift factor a_T, can also be applied to different compounds by using the measured glass transition temperature $T_{\rm g}$ in the expression for a_T'. Using this formalism we obtain very good agreement between theory and experiment for all studied systems.

The comparison of dry rubber friction with experiments presented so far needs to be extended. Note that in all the tests of the theory, we have only probed the adhesive contribution to the friction on the rising side of the $\mu_{\rm cont}(v)$-curve. However, for tire application the higher velocity side where $\mu_{\rm cont}(v)$ decreases with increasing v is more important. To check the theory in this case (at so low sliding speeds that frictional heating can be neglected) we need to perform sliding friction experiments at lower temperatures than possible with the present set-up (where the lowest temperature is $\approx -6\,^{\circ}$C). For this reason, we need to build another friction instrument and perform friction studies at lower temperatures (maybe down to $-50\,^{\circ}$C) to test the theory.

ACKNOWLEDGMENTS

The research work was performed within a Reinhart-Koselleck project funded by the Deutsche Forschungsgemeinschaft (DFG). The authors would like to thank DFG for the project support under the reference German Research Foundation DFG-Grant No. MU 1225/36-1. This work is supported in part by COST Action MP1303.

[1]B. N. J. Persson, *Sliding Friction: Physical Principles and Applications*, 2nd ed. (Springer, Heidelberg, 2000).
[2]K. Vorvolakos and M. K. Chaudhury, Langmuir **19**, 6778 (2003).
[3]K. A. Grosch, Proc. R. Soc. A **274**, 21 (1963).
[4]K. A. Grosch, Rubber Chem. Technol. **69**, 495 (1997).
[5]*The Pneumatic Tire*, edited by A. N. Gent and J. D. Walter (U.S. Department of Transportation, 2006).
[6]H. B. Pacejka, *Tyre and Vehicle Dynamics*, 2nd ed. (Elsevier, Amsterdam, 2006).
[7]B. N. J. Persson, J. Chem. Phys. **115**, 3840 (2001).
[8]B. N. J. Persson, J. Phys.: Condens. Matter **18**, 7789 (2006).
[9]G. Heinrich, M. Klüppel, and T. A. Vilgis, Comput. Theor. Polym. Sci. **10**, 53 (2000).
[10]G. Heinrich and M. Klüppel, Wear **265**, 1052 (2008).
[11]M. Klüppel and G. Heinrich, Rubber Chem. Technol. **73**, 578 (2000).
[12]S. Westermann, F. Petry, R. Boes, and G. Thielen, Kautsch. Gummi Kunstst. **57**, 645 (2004).
[13]B. N. J. Persson and A. I. Volokitin, Eur. Phys. J. E **21**, 69 (2006).
[14]G. Carbone, B. Lorenz, B. N. J. Persson, and A. Wohlers, Eur. Phys. J. E **29**, 275 (2009).
[15]B. N. J. Persson, Surf. Sci. **401**, 445 (1998).
[16]A. Le Gal and M. Klüppel, J. Chem. Phys. **123**, 014704 (2005).
[17]B. N. J. Persson, J. Phys.: Condens. Matter **21**, 485001 (2009).
[18]M. Mofidi, B. Prakash, B. N. J. Persson, and O. Albohr, J. Phys.: Condens. Matter **20**, 085223 (2008).
[19]B. N. J. Persson, O. Albohr, U. Tartaglino, A. I. Volokitin, and E. Tosatti, J. Phys.: Condens. Matter **17**, R1 (2005).
[20]B. N. J. Persson, O. Albohr, C. Creton, and V. Peveri, J. Chem. Phys. **120**, 8779 (2004).
[21]B. N. J. Persson, J. Phys.: Condens. Matter **23**, 015003 (2011).
[22]B. N. J. Persson, Eur. Phys. J. E **33**, 327 (2010).
[23]B. Lorenz, B. N. J. Persson, S. Dieluweit, and T. Tada, Eur. Phys. J. E **34**, 129 (2011).
[24]B. Lorenz, B. N. J. Persson, G. Fortunato, M. Giustiniano, and F. Baldoni, J. Phys.: Condens. Matter **25**, 095007 (2013).
[25]G. Carbone and C. Putignano, Phys. Rev. E **89**, 032408 (2014).
[26]B. N. J. Persson, N. Prodanov, B. A. Krick, N. Rodriguez, N. Mulakaluri, W. G. Sawyer, and P. Mangiagalli, Eur. Phys. J. E **35**, 5 (2012).
[27]B. Lorenz, N. Rodriguez, P. Mangiagalli, and B. N. J. Persson, Eur. Phys. J. E **37**, 57 (2014).
[28]I. Sivebaek, V. Samolilov, and B. N. J. Persson, Phys. Rev. Lett. **108**, 036102 (2012).
[29]I. Sivebaek, V. Samolilov, and B. N. J. Persson, Eur. Phys. J. E **27**, 37 (2008).
[30]S. Yamada, Tribol. Lett. **13**, 167 (2002).
[31]A. Schallamach, Wear **6**, 375 (1963).
[32]B. N. J. Persson and A. I. Volokitin, Eur. Phys. J. E **21**, 69 (2006).
[33]H. J. Park, C. Son, and S. H. Park, Int. J. Precis. Eng. Manuf. **15**, 2469 (2014).
[34]B. N. J. Persson, Tribol. Lett. **54**, 99 (2014).
[35]B. Lorenz, W. Pyckhout-Hintzen, and B. N. J. Persson, Polymer **55**, 565 (2014).
[36]In the non-linear response region, if the applied strain oscillates as $\epsilon(t) = \epsilon_0 \cos(\omega t)$, the stress will be a sum involving terms $\sim \cos(n\omega t)$ and $\sim \sin(n\omega t)$, where n is an integer. The DMA instrument we use defines the modulus $E(\omega)$ in the non-linear region using only the component $f(\epsilon_0,\omega)\cos(\omega t) + g(\epsilon_0,\omega)\sin(\omega t)$ in this sum which oscillates with the same frequency as the applied strain. Thus, $\mathrm{Re}E(\omega) = f(\epsilon_0,\omega)/\epsilon_0$ and $\mathrm{Im}E(\omega) = g(\epsilon_0,\omega)/\epsilon_0$. Note that with this definition the dissipated energy during one period of oscillation ($T = 2\pi/\omega$) is $\int_0^T dt\sigma(t)\dot{\epsilon}(t) = \pi\epsilon_0^2 \mathrm{Im}E(\omega)$ just as in the linear response region.
[37]A. Almqvist, C. Campana, N. Prodanov, and B. N. J. Persson, J. Mech. Phys. Solids **59**, 2355 (2011).
[38]B. N. J. Persson, Phys. Rev. Lett. **99**, 125502 (2007).
[39]C. Yang and B. N. J. Persson, J. Phys.: Condens. Matter **20**, 215214 (2008).
[40]M. Scaraggi and B. N. J. Persson, J. Phys.: Condens. Matter **27**, 105102 (2015).
[41]The Persson contact mechanics theory is a small-slope theory and it is not clear *a priori* how accurate the predictions are for the rms slope 1.3. However, a recent study of Scaraggi *et al.* (unpublished) shows that the small slope approximation is accurate also for surfaces with rms slope of order 1.

[42]N. V. Rodriguez, M. A. Masen, and D. J. Schipper, Proc. Inst. Mech. Eng., Part J **227**, 398 (2012).
[43]B. A. Krick, J. R. Vail, B. N. J. Persson, and W. G. Sawyer, Tribol. Lett. **45**, 185 (2012).
[44]G. Carbone and L. Mangialardi, J. Mech. Phys. Solids **52**, 1267 (2004).
[45]See article about rubber friction by K. A. Grosch in Ref. 5.
[46]B. Lorenz and B. N. J. Persson (unpublished data).
[47]M. L. Williams, R. F. Landel, and J. D. Ferry, J. Am. Chem. Soc. **77**, 3701 (1955).
[48]It is not clear that the smooth surfaces used by Grosch (and other scientists) are really atomically smooth. Thus, for example, if a glass surface is prepared by cooling a liquid below the glass transition temperature, frozen capillary waves will exist on the surface which may generate a relative large rms slope and which will contribute to the viscoelastic rubber friction. See, e.g., B. N. J. Persson, Surf. Sci. Rep. **61**, 201 (2006) for a discussion about this point.
[49]A. Lang and M. Klüppel, "Temperature and Pressure dependence of the friction properties of tire tread compounds on rough granite," in *KHK 11th Fall Rubber Colloquium* (2014).
[50]A. N. Gent, Langmuir **12**, 4492 (1996).
[51]B. N. J. Persson and E. Brener, Phys. Rev. E **71**, 036123 (2005).
[52]B. N. J. Persson, O. Albohr, G. Heinrich, and H. Ueba, J. Phys.: Condens. Matter **17**, R1071 (2005).
[53]G. Carbone and B. N. J. Persson, Eur. Phys. J. E **17**, 261 (2005).
[54]K. G. Rowe, A. I. Bennet, B. A. Krick, and W. G. Sawyer, Tribol. Int. **62**, 208 (2013).